Rapid Communications

Constraining the Λ-nucleus potential within the Liège intranuclear cascade model

J. L. Rodríguez-Sánchez,[1,2,*] J.-C. David,[3] J. Hirtz,[3,4] J. Cugnon,[5] and S. Leray[3]
[1]*Universidad de Santiago de Compostela, E-15782 Santiago de Compostela, Spain*
[2]*GSI-Helmholtzzentrum für Schwerionenforschung GmbH, D-64291 Darmstadt, Germany*
[3]*IRFU, CEA, Université Paris-Saclay, F-91191 Gif-sur-Yvette, France*
[4]*Center for Space and Habitability, Universität Bern, CH-30 12 Bern, Switzerland*
[5]*Department of Astrophysics, Geophysics, and Oceanography, University of Liège, Allée du 6 août 19, Bâtiment B5, B-4000 Liège, Belgium*

(Received 12 June 2018; revised manuscript received 31 July 2018; published 16 August 2018)

The new version of the Liège intranuclear-cascade model (INCL), recently extended to the production of strange particles and hypernuclei, is used to investigate the Λ-nucleus potential in a broad range of nuclear masses from Si to Pb. The combination of the INCL calculation results with experimental cross sections of Λ hypernuclei, obtained from (π^+, K^+) reaction studies, allows us to constrain the Λ-nucleus potential depth with an accuracy of about 0.9 MeV. Our results show that the potential depth increases with the mass number (A) from 28 MeV in the region of medium-mass hypernuclei up to a maximum of 39.6 MeV in the region of heavy hypernuclei around $A = 208$. This deviation could be related to the nucleon-isospin dependence of the three-body Λ-nucleon-nucleon force in asymmetry matter whose contribution is more relevant in hyperneutron matter due to a strong contribution from Λnn interactions.

DOI: 10.1103/PhysRevC.98.021602

The experimental study of hypernuclei is one of the few possibilities to obtain information about nucleon-hyperon (NY), hyperon-hyperon (YY), and hyperon-nucleon-nucleon (YNN) forces, which have a high impact in astrophysical applications [1–6]. For some years NY potentials fitted to the existing experimental data on elastic NY scattering have been available for the theoretical description of hypermatter and hypernuclei [7]. Unfortunately, since the experimental data are rather scarce in comparison with the nucleon-nucleon case, the corresponding potentials are not very constrained [8–10]. In the case of YY and YNN forces the situation is even more complicated because there are no available data.

Experimental data from emulsion studies provided the first measurements of binding energies for light hypernuclei [11]. These experimental findings were followed by many theoretical studies that were aiming at determining the potential-well depth of Λ particles in nuclear matter. On the one hand, in the first phenomenological studies based on a Woods-Saxon potential well, it was found that a potential depth of about 30 MeV could provide a reasonable description of the data [12]. Subsequent phenomenological investigations showed that a multiparameter fit of binding energies changing the nuclear radius and the Λ-nucleus potential gives a better agreement, obtaining a potential well with a depth of about 28 MeV [13,14]. On the other hand, from more sophisticated models based on Brueckner-Hartree-Fock [9], Skyrme-Hartree-Fock [15], or soft-core one-boson exchange [8] approaches the potential depth could fluctuate between 21 and 35 MeV. However, these studies were only carried out for light- and medium-mass hypernuclei because of the scarce measurements of heavy hypernuclei.

In past decades, the strangeness-exchange reactions (π^+, K^+) and (K^-, π^-) were also utilized for the spectroscopic study of hypernuclei using the excitation spectra to extract information about the Λ-shell structure, obtaining the binding energies of Λ-single-particle states with an uncertainty of less than 2 MeV [16–19]. In the case of (π^+, K^+) reactions, the cross sections were also determined with an uncertainty of less than 7%.

In this Rapid Communication, we propose to study the Λ-nucleus potential depth by combining experimental data of hypernuclei produced in strangeness-exchange (π^+, K^+) reactions with theoretical calculations performed with sophisticated dynamical reaction models based on the intranuclear-cascade (INC) approach [20–24]. In these models, the reaction is described by means of a two-step process usually applied in spallation, fragmentation, and charge-exchange reactions [25–27]: The collision itself where part of the nucleons contained in the target nucleus are removed or modified and some excitation energy and angular momenta are gained by the remnant and subsequent deexcitation processes by evaporation of particles or, if applicable, by fission. Here, INC models are considered as a Monte Carlo method to solve numerically the dynamic transport equations describing the hadron-nucleus collision. The nature of INC models is essentially classical, being assumed that nucleons are perfectly localized in phase space and that they are bound by a potential. In this approach, the nuclear reaction process is treated as successive relativistic binary hadron-hadron collisions separated in time where the positions and momenta of the hadrons are followed as time evolves. It is also assumed that hadrons move along straight trajectories until they undergo a collision with another hadron or until they reach the surface where they could eventually escape. Cross sections are determined from a set of collision events taken at different impact parameters and for which nucleon positions

*Corresponding author: joseluis.rodriguez.sanchez@usc.es

and momenta are initially sampled for each participant nucleus.

For our purpose, we use the Liège intranuclear-cascade model (INCL) [28] that has been recently extended towards high energies ($\approx$15 GeV) including multipion production [29,30], strange particles, such as kaons and hyperons [31,32], and the production of η and ω mesons [33]. This new version of the INCL allows us to predict the formation of hyperremnants and their characterization in atomic, mass, and strange numbers together with their excitation energies and angular momenta. These improvements in INCL also require deexcitation models considering the emission of hyperons, in particular, the evaporation of Λ particles. Currently, there are a few numbers of deexcitation models that treat the evaporation of hyperons and the formation of hypernuclei. In this Rapid Communication we use the evaporation model ABLA07 developed at GSI by Kelić and collaborators [34], recently extended to hypernuclei by us including the evaporation of Λ particles on the basis of Weisskopf's approach according to Ref. [35].

In the new version of the INCL elementary cross sections related to the production and interaction of strange particles (such as K, $\bar{K}$, Σ, and Λ) were implemented using sophisticated parametrizations of available experimental data as well as their characteristics: angular distributions, momenta, and charge repartition of the particles in the associated final states [31,32]. These new ingredients made the INCL become a powerful tool to study the production of strange particles in nuclear matter and to go further in the understanding of hypernuclei formation.

Target density profiles are prepared at the first step of the simulation assuming independent Woods-Saxon density distributions for protons and neutrons according to the method described in Ref. [36]. For the Woods-Saxon density distribution the radius (R_0) and the diffuseness parameter (a) are taken from Hartree-Fock-Bogoliubov calculations since they provide a good description of single-nucleon knockout reactions [37]. The initial nucleon momenta are uniformly distributed in hard Fermi spheres of radii $(2Z/A)^{1/3}p_F$ for protons and $(2N/A)^{1/3}p_F$ for neutrons (see Ref. [38] for details). Moreover, the nucleons are sampled in phase space taking into account the correlations between the kinetic energy and the radius of the potential well [36]. The relation is such that the space density distribution is given by the Woods-Saxon distribution. For Λ particles we also use a Woods-Saxon potential well taking the diffuseness parameter (a_Λ) as for neutrons and a nuclear radius $R_0^\Lambda = (1.128 + 0.439A^{-2/3})A^{1/3}$ since this parametrization provides a reasonable description of the distance between hypernuclei binding energies [13]. In Table I are summarized the nuclear radii utilized to define the Woods-Saxon potential well of neutrons, protons, and Λ particles. In the case of Σ particles the nuclear radius is not defined since its potential is repulsive and therefore this particle is always emitted at the end of the cascade process. Finally, the Σ- and Λ-nucleus potential wells are set to constant values of 16 (repulsive) and 28 (attractive) MeV by default according to Refs. [39] and [13], respectively, although the Λ-nucleus potential will be modified later to constrain its depth within the strangeness-exchange (π^+, K^+) reactions.

For the dynamical description of the collision between projectile and target nuclei, each event is fired at a given impact parameter b, ranging from 0 to a distance $b_{\max}$ given by the maximum radius of the target nucleus. If two hadrons approach each other at a distance shorter than a minimum distance, they interact. The minimum distance is calculated from energy-dependent parametrizations of the hadron-hadron interaction cross sections for all possible collisions according to Ref. [40]. During the cascade process, the particles are divided into participants and spectators. Participants are defined as particles that have collided with at least one other participant, whereas spectators are the other particles. Collisions between spectators are forbidden in order to eliminate the spontaneous boiling of the Fermi sea, which leads to particles that could escape from the target, even if the particle is left alone. This condition is used because the spontaneous boiling is a direct violation of the Pauli-exclusion principle. For nucleons, a strict Pauli blocking is also applied to the first collision to account for surface effects and for effects of the depletion of the Fermi sea [41]. For the subsequent collisions, we apply the Pauli blocking according to the usual procedure by means of statistical blocking factors, which do not have any effect in the case of single-Λ hypernuclei. In addition, a consistent dynamical Pauli blocking is applied to all particles at the end of the cascade process to reject unphysical results, see Ref. [36] for more details. The excitation energy of the remnants is calculated from energy and momentum conservation laws applied over all existing particles in the initial configuration and at the end of the cascade process [36].

TABLE I. Nuclear radii (in femtometers) for neutrons, protons, and Λ's used in the INCL to define the Woods-Saxon potential well of the nuclei investigated in this Rapid Communication as well as the separation energies (in MeV) used in the deexcitation process.

Nucleus	R_n	R_p	R_Λ	S_n	S_p	S_Λ
${}^{28}_{\Lambda}$Si	3.25	3.29	3.57	16.00	10.30	16.0
${}^{89}_{\Lambda}$Y	5.01	4.84	5.13	9.55	6.51	22.1
${}^{139}_{\Lambda}$La	5.85	5.83	5.93	7.04	5.87	23.8
${}^{208}_{\Lambda}$Pb	6.76	6.64	6.76	5.88	7.74	26.5

In Fig. 1 we display the kinetic energy of the positive kaons emerged from the reaction $\pi^+(1.06\ \text{GeV}/c) + {}^{28}$Si producing hyperremnants of ${}^{28}_{\Lambda}$Si; this means that in this picture we do not take into account the deexcitation stage in which the excited hyperremnant could evaporate any particle. Here, the vertical lines indicate the angular selection of hyperremnants that will then enter the evaporation stage since the kaon emission angle is not affected by the deexcitation process.

For modeling the deexcitation stage, we use the ABLA07 code [34] that describes the deexcitation of a nucleus emitting γ rays, neutrons, light-charged particles, and intermediate-mass fragments according to Weisskopf's formalism [42]. For a more realistic description of this process, the separation energies are taken from the atomic mass evaluation of 2016 [43], and the emission barriers for charged particles are determined with the Bass potential [44]. This model has been extended by us to account for the emission of Λ particles and the production of cold hypernuclei, close to what has also been performed in Refs. [35,45]. The Λ-separation energies

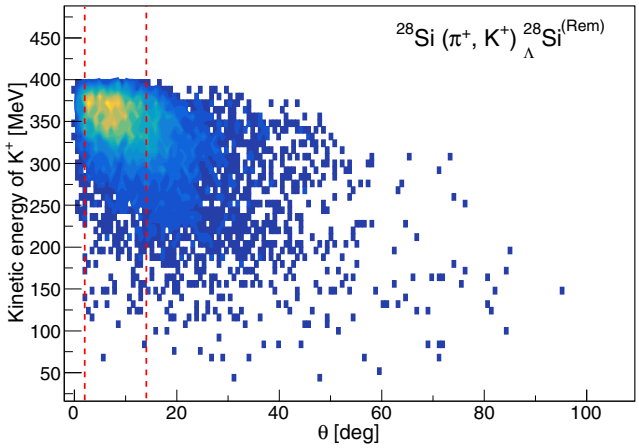

FIG. 1. Scatter plot of the INCL predictions for the kinetic energy of K^+ particles emitted in the production of hyperremnants $^{28}_{\Lambda}\mathrm{Si}^{(\mathrm{Rem})}$ as a function of angle θ for the reaction $\pi^+(1.06\ \mathrm{GeV}/c) + {}^{28}\mathrm{Si}$. The vertical lines located at 2° and 14° are to indicate the hyperremnants selected to enter the evaporation stage.

are parametrized according to the fit of experimental binding energies described in Ref. [46]. In addition, neutron and proton separation energies are modified in the case of hypernuclei to take into account the hyperenergy released from the presence of the Λ particle [45]. The values of all the separation energies used in this Rapid Communication are also listed in Table I. For this specific Rapid Communication, we do not need to introduce more ingredients in the deexcitation process since we are only interested in the survival probability of the isobaric hyperremnant that is determined basically by the number of excited hyperremnants with an excitation energy that does not go beyond the minimum particle-separation energy, defined as $S_{\min} = \min\{S_n, S_p, S_\Lambda\}$. This probability can be written as

$$P_{E^* \leqslant S_{\min}} = \frac{1}{N} \sum_{j=0}^{N} \Theta(S_{\min} - E_j^*),$$

where Θ is the Heaviside function and N is the total number of isobaric hyperremnants produced by strangeness-exchange reactions. Finally, the cross section of the isobaric strangeness-exchange hypernuclei will be used to study and constrain the Λ potential as explained below.

In Fig. 2 we show the results obtained from our calculations for the strangeness-exchange reactions indicated in each panel. In these pictures we illustrate how the cross section evolves with the Λ-nucleus potential depth. One can see that the cross sections increase with the Λ potential, which is basically explained by the increase in the phase space compatible with the kinetic energy gained by the Λ particle. After defining these correlations for each hypernucleus, we can use the experimental cross sections, indicated in the figure with vertical dashed lines, to constrain the Λ-nucleus potential depth.

Our findings for the Λ-nucleus potential depth (open squares) are displayed in Fig. 3 together with the results obtained in other works. For hypernuclei with mass numbers below 89 we obtain a potential depth of around 28 MeV that is

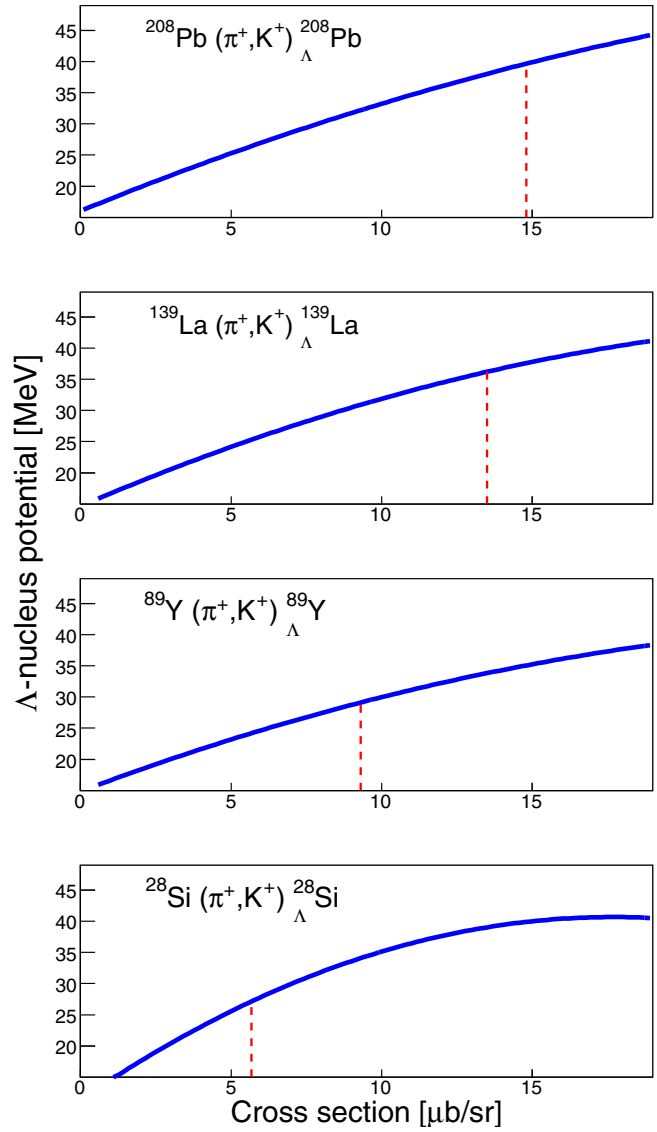

FIG. 2. Correlation between the Λ-nucleus potential and the cross section of hypernuclei produced in the reactions indicated in each panel for a pion momentum of 1.06 GeV/c. The vertical lines indicate the experimental cross sections, obtained from Ref. [17], that were used to determine the potential-well depth.

in agreement with the values reported in other works based on phenomenological approaches [13] and on Skyrme-Hartree-Fock calculations [15]. However, for higher masses we find a potential depth of 36.2 MeV for $^{139}_{\Lambda}$La and 39.6 MeV for $^{208}_{\Lambda}$Pb, which were not observed in previous investigations because of the scarce experimental measurements in the region of heavy hypernuclei. We also performed INCL calculations assuming a smaller phenomenological radius of $R_0^\Lambda = 1.165A^{1/3}$ suggested by Gal and collaborators [47], which leads to a lower Λ-potential depth for Pb of about 37 MeV, but this value is still far from being adequate according to other theoretical predictions, and thus it cannot explain the observed deviation. Recently, some works have also pointed out this possible deviation [10] whose understanding is still not clear.

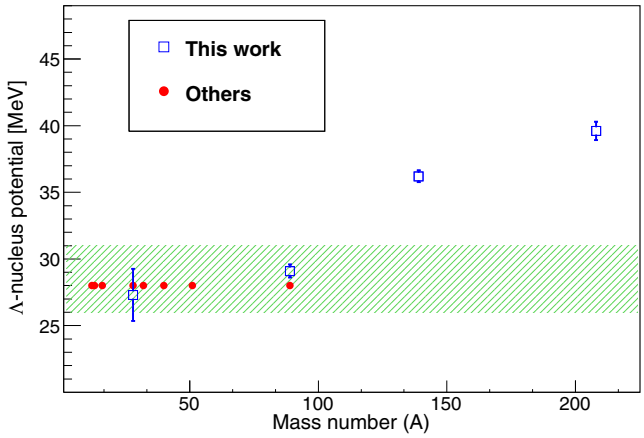

FIG. 3. Λ-nucleus potential obtained from our model calculations (open squares) compared with the values reported in other works (solid circles). The dashed area is just to show the expected region for the Λ-potential depth.

To go further, in Fig. 4 we also display the Λ-nucleus potential depth as a function of the asymmetry of the target nucleus, defined as $(N-Z)/A$, where N is the number of neutrons, Z is the number of protons, and A is the mass number. This asymmetry parameter was proposed recently by Lonardoni and Pederiva [48] to study the nucleon-isospin dependence of the three-body ΛNN force in neutron-rich hypermatter that could be important for the prediction of neutron star properties, although the conclusions drawn from that work are still under debate since the Σ particle as well as the ΛN and ΣN couplings were not considered. In this sense, our calculations take into account these channels, which were introduced in our model through the parametrization of the existing elementary cross sections [31]. In the picture, we can observe a strong increase in the Λ-potential depth with the asymmetry parameter when we move towards neutron-rich nuclei, which have a large neutron abundance at the surface that

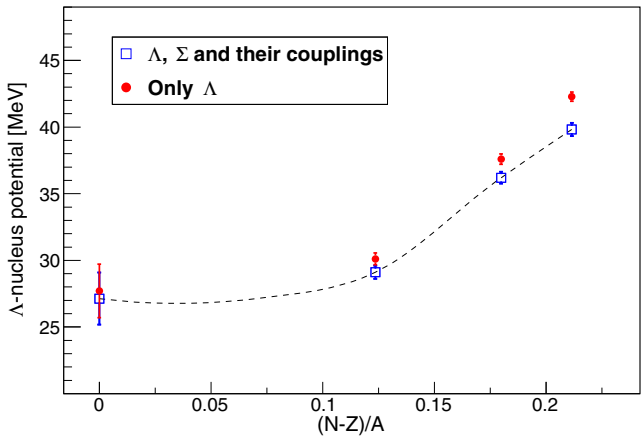

FIG. 4. Λ-nucleus potential obtained from our approach as a function of the asymmetry $(N-Z)/A$ (open squares). The dashed line is just a guide to the eye. The solid circles also refer to our calculations but inhibiting the presence of the Σ particle.

enhances the Λnn interaction. Here, we also show a calculation without considering the production and absorption of the Σ particle (solid circles) to understand its role in the constraint of the Λ-nucleus potential depth. As can be seen, the presence of the Σ particle and its couplings are more important in the region of neutron-rich nuclei, reducing in around 3 MeV the Λ-nucleus potential depth of ${}^{208}_{\Lambda}$Pb. Nevertheless, both calculations lead to an increase in the potential depth with the asymmetry of the nucleus, and therefore, this deviation can tentatively be attributed to a strong Λnn interaction. Note that in our INCL calculations we do not take into account three-body collisions, but it is clearly evident that their effects are included in the experimental separation energies and cross sections that we use as an input in our approach. Therefore, the deviation that we find in Figs. 3 and 4 could be considered as the first strong hint of such dependence that should be investigated in detail.

It is sometimes difficult to find evident numerical implications about one parameter in the results of a multiparametric model. But in our case, we think that our conclusions are rather strong because the formation of hypernuclei depends only on the creation and propagation of hyperons, mainly Λ and Σ particles, inside nuclear matter. These features are embodied by the elementary strangeness cross section, which is well known, and by the average Λ-nucleus potential, which are thus not really sensitive to the parameters of the nonstrange sector.

In conclusion, a new version of INCL has been used for the first time to investigate the production of hypernuclei in strangeness-exchange collisions. The INCL calculations that account for the production and absorption of the Λ and Σ particles together with experimental Λ-separation energies are utilized to establish direct correlations between the cross sections of hypernuclei produced via the strangeness-exchange reactions (π^+, K^+) and the Λ-nucleus potential depth. Experimental cross sections are then used to determine the potential depth with an average accuracy of 0.9 MeV. These constraints provide a potential depth of about 28 MeV for medium-mass hypernuclei that is consistent with the results obtained in other works, whereas for heavy hypernuclei around Pb, we obtain a potential depth of 39.6 MeV. To go a step further in the interpretation, we also investigate how the Λ-nucleus potential depth evolves with the asymmetry of the nucleus. Surprisingly, we find a strong increase in the Λ-nucleus potential depth when we move towards neutron-rich nuclei. This deviation cannot be explained by the ΣN-ΛN couplings during the cascade process, and thus, we conclude that this fact could be a first indication of a strong Λnn interaction in neutron-rich matter. We also think that more measurements in the region of heavy hypernuclei and theoretical analysis should be performed in order to confirm and understand this interesting behavior.

We wish to thank Dr. A. Boudard, Dr. D. Mancusi for enlightening discussions, and Dr. G. Schnabel for his technical support. This work has been partially supported by the Department of Education, Culture and University Organization of the Regional Government of Galicia under the Program of Postdoctoral Fellowships and by the EU ENSAR2 FP7 Project (Grant Agreement No. 654002).

[1] I. Vidaña, A. Polls, A. Ramos, L. Engvik, and M. Hjorth-Jensen, Phys. Rev. C **62**, 035801 (2000).
[2] D. Lonardoni, A. Lovato, S. Gandolfi, and F. Pederiva, Phys. Rev. Lett. **114**, 092301 (2015).
[3] A. I. Qauli, M. Iqbal, A. Sulaksono, and H. S. Ramadhan, Phys. Rev. D **93**, 104056 (2016).
[4] R. Wirth and R. Roth, Phys. Rev. Lett. **117**, 182501 (2016).
[5] M. Fortin, S. S. Avancini, C. Providência, and I. Vidaña, Phys. Rev. C **95**, 065803 (2017).
[6] Y. Yamamoto, T. Furumoto, N. Yasutake, and T. A. Rijken, Phys. Rev. C **88**, 022801(R) (2013); **90**, 045805 (2014); Eur. Phys. J. A **52**, 19 (2016).
[7] K. Tominaga, T. Ueda, M. Yamaguchi, N. Kijima, D. Okamoto, K. Miyagawa, and T. Yamada, Nucl. Phys. **A642**, 483 (1998).
[8] T. A. Rijken, V. G. J. Stoks, and Y. Yamamoto, Phys. Rev. C **59**, 21 (1999).
[9] H.-J. Schulze, M. Baldo, U. Lombardo, J. Cugnon, and A. Lejeune, Phys. Rev. C **57**, 704 (1998).
[10] H.-J. Schulze and T. Rijken, Phys. Rev. C **88**, 024322 (2013).
[11] D. H. Davis and J. Pniewski, Contemp. Phys. **27**, 91 (1986).
[12] C. B. Dover, L. Ludeking, and G. E. Walker, Phys. Rev. C **22**, 2073 (1980).
[13] D. J. Millener, C. B. Dover, and A. Gal, Phys. Rev. C **38**, 2700 (1988).
[14] A. Bouyssy and J. Hüfner, Phys. Lett. **64B**, 276 (1976).
[15] J. Cugnon, A. Lejeune, and H.-J. Schulze, Phys. Rev. C **62**, 064308 (2000).
[16] R. Bertini *et al.*, Phys. Lett. **83B**, 306 (1979); Nucl. Phys. **A360**, 315 (1981).
[17] T. Hasegawa, O. Hashimoto, S. Homma, T. Miyachi, T. Nagae, M. Sekimoto, T. Shibata, H. Sakaguchi, T. Takahashi, K. Aoki, H. Noumi, H. Bhang, M. Youn, Y. Gavrilov, S. Ajimura, T. Kishimoto, A. Ohkusu, K. Maeda, R. Sawafta, and R. P. Redwine, Phys. Rev. C **53**, 1210 (1996).
[18] P. H. Pile, S. Bart, R. E. Chrien, D. J. Millener, R. J. Sutter, N. Tsoupas, J.-C. Peng, C. S. Mishra, E. V. Hungerford, T. Kishimoto, L.-G. Tang, W. von Witsch, Z. Xu, K. Maeda, D. Gill, R. McCrady, B. Quinn, J. Seydoux, J. W. Sleight, R. L. Stearns, H. Plendl, A. Rafatian, and J. Reidy, Phys. Rev. Lett. **66**, 2585 (1991).
[19] P. K. Saha, T. Fukuda, W. Imoto, J. K. Ahn, S. Ajimura, K. Aoki, H. C. Bhang, H. Fujioka, H. Hotchi, J. I. Hwang, T. Itabashi, B. H. Kang, H. D. Kim, M. J. Kim, T. Kishimoto, A. Krutenkova, T. Maruta, Y. Miura, K. Miwa, T. Nagae, H. Noumi, H. Outa, T. Ohtaki, A. Sakaguchi, Y. Sato, M. Sekimoto, Y. Shimizu, H. Tamura, K. Tanida, A. Toyoda, M. Ukai, and H. J. Yim, Phys. Rev. Lett. **94**, 052502 (2005).
[20] H. W. Bertini, Phys. Rev. **131**, 1801 (1963); **188**, 1711 (1969).
[21] K. Chen, Z. Fraenkel, G. Friedlander, J. R. Grover, J. M. Miller, and Y. Shimamoto, Phys. Rev. **166**, 949 (1968).
[22] Y. Yariv and Z. Fraenkel, Phys. Rev. C **20**, 2227 (1979).
[23] V. S. Barashenkov, B. F. Kostenko, and A. M. Zadorogny, Nucl. Phys. **A338**, 413 (1980).
[24] J. Cugnon, Phys. Rev. C **23**, 2094 (1981).
[25] R. Serber, Phys. Rev. **72**, 1114 (1947).
[26] A. Boudard, J. Cugnon, J.-C. David, S. Leray, and D. Mancusi, Phys. Rev. C **87**, 014606 (2013).
[27] Th. Aoust and J. Cugnon, Phys. Rev. C **74**, 064607 (2006).
[28] D. Mancusi, A. Boudard, J. Cugnon, J.-C. David, P. Kaitaniemi, and S. Leray, Phys. Rev. C **90**, 054602 (2014).
[29] S. Pedoux, J. Cugnon, A. Boudard, J.-C. David, and S. Leray, Adv. Space Res. **44**, 926 (2009).
[30] D. Mancusi, S. Lo Meo, N. Colonna, A. Boudard, M. A. Cortés-Giraldo, J. Cugnon, J.-C. David, S. Leray, J. Lerendegui-Marco, C. Massimi, and V. Vlachoudis, Eur. Phys. J. A **53**, 80 (2017).
[31] J. Hirtz, J.-C. David, A. Boudard, J. Cugnon, S. Leray, and D. Mancusi, https://arxiv.org/abs/1805.01655.
[32] J. Hirtz *et al.* (unpublished).
[33] J.-C. David, A. Boudard, J. Cugnon, J. Hirtz, S. Leray, D. Mancusi, and J. L. Rodríguez-Sánchez, Eur. Phys. J. Plus **133**, 253 (2018).
[34] A. Kelić, M. V. Ricciardi, and K.-H. Schmidt, *Proceedings of Joint ICTP-IAEA Advanced Workshop on Model Codes for Spallation Reactions, ICTP Trieste, Italy, 2008* edited by D. Filges, S. Leray, Y. Yariv, A. Mengoni, A. Stanculescu, and G. Mank [IAEA INDC(NDS)-530, Vienna, 2008], pp. 181–221.
[35] A. S. Botvina, N. Buyukcizmeci, A. Ergun, R. Ogul, M. Bleicher, and J. Pochodzalla, Phys. Rev. C **94**, 054615 (2016).
[36] A. Boudard, J. Cugnon, S. Leray, and C. Volant, Phys. Rev. C **66**, 044615 (2002).
[37] J. L. Rodríguez-Sánchez, J.-C. David, D. Mancusi, A. Boudard, J. Cugnon, and S. Leray, Phys. Rev. C **96**, 054602 (2017).
[38] D. Mancusi, A. Boudard, J. Carbonell, J. Cugnon, J.-C. David, and S. Leray, Phys. Rev. C **91**, 034602 (2015).
[39] T. A. Rijken and H.-J. Schulze, Eur. Phys. J. A **52**, 21 (2016).
[40] J. Cugnon, D. L'Hôte, and J. Vandermeulen, Nucl. Instrum. Methods Phys. Res., Sect. B **111**, 215 (1996).
[41] J. Cugnon and P. Henrotte, Eur. Phys. J. A **16**, 393 (2003).
[42] V. F. Weisskopf and D. H. Ewing, Phys. Rev. **57**, 472 (1940).
[43] W. J. Huang, G. Audi, M. Wang, F. G. Kondev, S. Naimi, and X. Xu, Chin. Phys. C **41**, 030002 (2017).
[44] R. Bass, *Proceedings of the Symposium on Deep-Inelastic and Fusion Reactions with Heavy Ions* (Springer-Verlag, Berlin, 1980).
[45] N. Buyukcizmeci, A. S. Botvina, J. Pochodzalla, and M. Bleicher, Phys. Rev. C **88**, 014611 (2013).
[46] C. Samanta, P. Roy Chowdhury, and D. N. Basu, J. Phys. G.: Nucl. Part. Phys. **32**, 363 (2006).
[47] A. Gal, E. V. Hungerford, and D. J. Millener, Rev. Mod. Phys. **88**, 035004 (2016).
[48] D. Lonardoni and F. Pederiva, https://arxiv.org/abs/1711.07521.